Available online at www.sciencedirect.com
ScienceDirect
Acta Materialia 55 (2007) 4409–4418
Acta MATERIALIA
www.elsevier.com/locate/actamat

La-based bulk metallic glasses with critical diameter up to 30 mm

Q.K. Jiang [a], G.Q. Zhang [a,b], L. Yang [a], X.D. Wang [a], K. Saksl [c], H. Franz [c], R. Wunderlich [d], H. Fecht [d,e], J.Z. Jiang [a,*]

[a] International Center for New-Structured Materials (ICNSM) and Laboratory of New-Structured Materials, Department of Materials Science and Engineering, Zhejiang University, Hangzhou 310027, China
[b] Key Laboratory of Advanced Textile Materials and Manufacturing Technology, Zhejiang Sci-Tech University, Hangzhou 310018, China
[c] HASYLAB am DESY, Notkestrasse 85, D-22603 Hamburg, Germany
[d] Department of Materials, Faculty of Engineering, University of Ulm, Albert-Einstein Allee 47, D-89081 Ulm, Germany
[e] Forschungszentrum Karlsruhe, Institut für Nanotechnologie, Karlsruhe, Germany

Received 22 January 2007; received in revised form 6 April 2007; accepted 9 April 2007
Available online 30 May 2007

Abstract

We report composition optimization, thermal and physical properties of new La-based bulk metallic glasses with high glass forming ability (GFA) based on a ternary $La_{62}Al_{14}Cu_{24}$ alloy. By refining the (Cu, Ag)/(Ni, Co) and La/(Cu, Ag) ratios in the La–Al–(Cu,Ag)–(Ni, Co) pseudo-quaternary alloy, the formation of 30 mm diameter of $La_{65}Al_{14}(Cu_{5/6}Ag_{1/6})_{11}(Ni_{1/2}Co_{1/2})_{10}$ bulk metallic glass (BMG) alloy is achieved using water quenching. The origin of the high GFA was investigated from the kinetic, structural and thermodynamic points of view, and was found to be due to the smaller difference in Gibbs free-energy between the amorphous and crystalline phases in the pseudo-quaternary alloy. These alloys exhibit low glass transition temperatures, below 430 K, and relatively wide supercooled liquid regions of 40–60 K. Mechanical tests on these alloys show a fracture strength of 650 GPa, Vicker's hardness 200 kg mm^{-2}, Young's modulus 35 GPa, shear modulus 13 GPa and Poisson ratio 0.356. The La-based BMGs are useful for both scientific and engineering applications.

Keywords: Glass forming ability; Bulk metallic glass; Water quenching; Thermodynamics; Structure

1. Introduction

Compared with crystalline counterparts, bulk metallic glasses (BMGs) have some superior properties, such as high yield strength, hardness, large elastic limit, high fracture toughness and corrosion resistance, and hence are considered as promising engineering materials [1–3]. However, one drawback that severely restricts their applications is their limited glass forming ability (GFA) since critical sizes (D_c) of BMGs of up to 20 mm [4] are usually required for structural materials. From this standpoint, only a few alloy systems based on Pd [5], Zr [6], Y [7] and Mg [4] can be considered candidates, though these have other problems.

Recently, rare earth (Re)-based BMGs have attracted more attention for their unique physical properties, such as the magnetic properties of the Nd- and Pr-based BMGs [8,9] and the polymer-like thermoplastic behavior of the Ce-based BMGs [10]. They also show relatively superior GFA, e.g. the centimeter-sized LaCe-based BMGs developed by Jiang et al. [11] and the 15 mm LaPrCeNd-based BMGs developed by Li et al. [12]. As such, developing inch-sized Re-based BMGs is desirable for both scientific significance and practical applications. La-based BMGs were found to be high glass formers first by Inoue et al. and then by Li et al. [13–16]. The largest sizes for forming glassy structures reported were 9 mm for $La_{55}Al_{25}Cu_{10}Ni_5Co_5$ alloys [13] and 12 mm for $La_{62}Al_{14}(Cu_{0.5}Ni_{0.5})_{24}$ alloys [15]. Recently, based on the simple $La_{62}Al_{14}Cu_{24}$ alloy, we have successfully developed a new composition of $La_{62}Al_{14}(Cu_{5/6}Ag_{1/6})_{14}Ni_5Co_5$ [17]. It can be fabricated into fully amorphous rods with diameters of at least 20 mm by substituting elements with similar chemical properties and similar atomic sizes [17]. As has been proved

* Corresponding author.
E-mail address: jiangjz@zju.edu.cn (J.Z. Jiang).

1359-6454/$30.00
doi:10.1016/j.actamat.2007.04.021

by experiments, the GFA of BMGs is sensitive to the composition of the alloys [4,15,16]. It is therefore expected that alloys with higher GFA could be found in the La–Al–(Cu, Ag)–(Ni, Co) pseudo-quaternary system by optimizing the alloys' compositions.

In this work, we report the formation of a series of La-based BMGs with diameters more than 20 mm. By refining the (Cu, Ag)/(Ni, Co) and La/(Cu, Ag) ratios in La–Al–(Cu, Ag)–(Ni, Co) pseudo-quaternary alloy system, we demonstrate the formation of 30 mm diameter BMGs using water quenching. To the best of our knowledge, this is the highest GFA in Re-based alloy systems reported so far. The origins of the excellent GFA enhanced by Ag and Ni–Co substitution are systematically investigated from the structural, thermodynamic and kinetic aspects. The thermal and mechanical properties and elastic constants for the developed La-based BMGs are also presented.

2. Experimental

Master ingots with nominal compositions of $La_{62}Al_{14}Cu_{24}$ and $La_{62}Al_{14}(Cu_{5/6}Ag_{1/6})_{24}$ were directly arc-melted in a Ti-gettered high-purity argon atmosphere. However, in order to obtain homogeneous ingots with nominal compositions of $La_{62}Al_{14}(Cu_{5/6}Ag_{1/6})_{24-x}(Ni_{0.5}Co_{0.5})_x$ ($x = 2, 4, 6, 8, 10$ and 12 at.%) and $La_yAl_{14}(Cu_{5/6}Ag_{1/6})_{76-y}(Ni_{1/2}Co_{1/2})_{10}$ ($y = 60, 62, 64, 65, 66$ and 68 at.%), we first made Cu–Ag–Ni–Co ingots, and then arc-melted the ingot together with La and Al to obtain the final desired compositions. The purities of the elements ranged from 99.5 to 99.98 at.%. The ingots were remelted at least four times to achieve chemical homogeneity. For smaller samples (diameter < 20 mm), the master alloys were further processed by suction-casting into copper molds under a purified argon atmosphere. For rods larger than 20 mm in diameter, the ingot was melted in a Ti-gettered high-purity argon atmosphere quartz container followed by water quenching. Copper molds with diameters of 2, 3, 8, 16 and 20 mm as well as quartz tubes ranging from 26 to 30 mm in diameter were used. The amorphous nature in the transverse cross-sections of the samples was verified by using a Thermo ARL X'Tra diffractometer with Cu Kα radiation at 45 kV.

Structural analysis of the as-prepared specimens was conducted using synchrotron radiation X-ray diffraction at the BW5 station of HASYLAB, Hamburg [18]. The beam size was 1×1 mm^2 and the wavelength used was 0.12398 Å. High-resolution X-ray diffraction (HRXRD) patterns with a large Q range, scanning a 30 mm disk of the $La_{65}Al_{14}(Cu_{5/6}Ag_{1/6})_{11}(Ni_{1/2}Co_{1/2})_{10}$ BMG, were recorded on an image plate (MAR 345, $150 \times 150\mu m^2$ pixel size). The scattering intensity $I(q)$ (vs. scattering vector) was determined using the software package FIT2D [19]. The structure factor $S(q)$ and the pair distribution function (PDF) $G(r)$ were obtained by PDFgetX2 [20].

A differential scanning calorimeter (NETZSCH DSC 404C) was used to detect the crystallization and melting behaviors of as-prepared BMGs under a continuous argon flow at a heating rate of 20 K min^{-1}. The specific heat capacity of the amorphous phase, the supercooled liquid phase and the crystalline phase was measured on a Perkin–Elmer DSC-7 by comparison with the specific heat capacity of a standard sapphire sample.

The Vickers hardness of as-prepared samples was measured under 200 g load by a Vickers diamond pyramidal microhardness tester (MH5, China) at room temperature. Cylindrical glassy rods, 2 mm in diameter and 4 mm in height, were used for compression tests, which were performed using a universal test machine controlled by computer (CMT5205 SANS, China). The acoustic longitudinal velocity (V_l) and shear velocity (V_s) of the $La_{62}Al_{14}(Cu_{5/6}Ag_{1/6})_{14}(Ni_{1/2}Co_{1/2})_{10}$ BMG were measured by a MATEC 6600 model ultrasonic system with a measuring sensitivity of 0.5 ns. The sample rod was cut to a length of 4 mm, and the ends were carefully polished in parallel. The carrying frequency of the ultrasonic is 5 MHz. Based on Archimedes' principle, density (ρ) measurements of the $La_{62}Al_{14}(Cu_{5/6}Ag_{1/6})_{14}(Ni_{1/2}Co_{1/2})_{10}$ BMG were performed with a Mettler Toledo XS105 microbalance having a sensitivity of 0.01 mg. The Young's modulus E, shear modulus G, bulk modulus K and Poisson's ratio σ were derived from the acoustic velocities and the density data using the following equations [21,22]:

$$G = \rho V_s^2 \tag{1}$$

$$K = \rho\left(V_l^2 - \frac{4}{3}V_s^2\right) \tag{2}$$

$$\sigma = \frac{(V_l^2 - 2V_s^2)}{2(V_l^2 - V_s^2)} \tag{3}$$

$$E = 2G(1 + \sigma) \tag{4}$$

3. Results

3.1. Pseudo-quaternary La–Al–(Cu, Ag)–(Ni, Co) alloys

Fig. 1 shows the XRD patterns of the $La_{62}Al_{14}(Cu_{5/6}Ag_{1/6})_{24-x}(Ni_{0.5}Co_{0.5})_x$ ($x = 0, 2, 4, 6, 8, 10$ and 12 at.%)

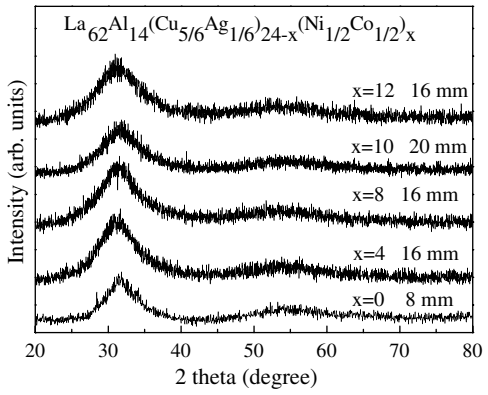

Fig. 1. XRD patterns of the $La_{62}Al_{14}(Cu_{5/6}Ag_{1/6})_{24-x}(Ni_{0.5}Co_{0.5})_x$ ($x = 0, 2, 4, 6, 8, 10$ and 12 at.%) glassy alloys.

glassy alloys. For the Ni–Co-free alloys, 8 mm is the upper limit for amorphous phase formation, while with a small amount of Ni–Co ($\leqslant$12 at.%) substitution, 16–20 mm fully amorphous alloys can be obtained. It was found that the alloy with $x = 10$ at.% shows the best GFA. We further studied the La/(Cu, Ag) ratio effect on the GFA of the alloys and found that the critical size of amorphous rods in $La_y Al_{14}(Cu_{5/6}Ag_{1/6})_{76-z}(Ni_{1/2}Co_{1/2})_{10}$ compositions can be distinctly enhanced by adjusting the y value. From XRD patterns in Fig. 2a, it is evident that, for the samples with $y = 62, 64$ and 66, the 20 mm rod samples are fully amorphous, while the 16 mm rod samples of the $La_yAl_{14}(Cu_{5/6}Ag_{1/6})_{76-y}(Ni_{1/2}Co_{1/2})_{10}$ ($y = 60$ and 68 at.%) pseudo-quaternary alloys are a mixture of amorphous and crystalline phases. For the alloys with D_c larger than 20 mm, water quenching was employed to evaluate their GFA, because the maximum size of our copper mold by sucking is 20 mm. The XRD patterns of 26 and 30 mm rods are presented in Fig. 2b. It can be seen that the $La_yAl_{14}(Cu_{5/6}Ag_{1/6})_{76-y}(Ni_{1/2}Co_{1/2})_{10}$ alloys ($y = 64$ and 66) exhibit an amorphous structure, while the 26 mm rod of the $La_{62}Al_{14}(Cu_{5/6}Ag_{1/6})_{14}(Ni_{1/2}Co_{1/2})_{10}$ alloy is partially crystallized. When the rod size was increased to 30 mm, only the $La_{65}Al_{14}(Cu_{5/6}Ag_{1/6})_{11}(Ni_{1/2}Co_{1/2})_{10}$ alloy could be quenched into a fully amorphous structure. Fig. 3a is a picture of the 30 mm amorphous rod for the $La_{65}Al_{14}(Cu_{5/6}Ag_{1/6})_{11}(Ni_{1/2}Co_{1/2})_{10}$ alloy prepared by water quenching. To further ascertain the glassy nature, high-resolution X-ray diffraction were performed for the 30 mm $La_{65}Al_{14}(Cu_{5/6}Ag_{1/6})_{11}(Ni_{1/2}Co_{1/2})_{10}$ alloy. Fig. 3b illustrates a schematic map of the scanned positions. No detectable crystalline peaks were detected for more than 40 HRXRD patterns recorded in Fig. 3c and d, confirming the fully amorphous structure of the 30 mm rod sample.

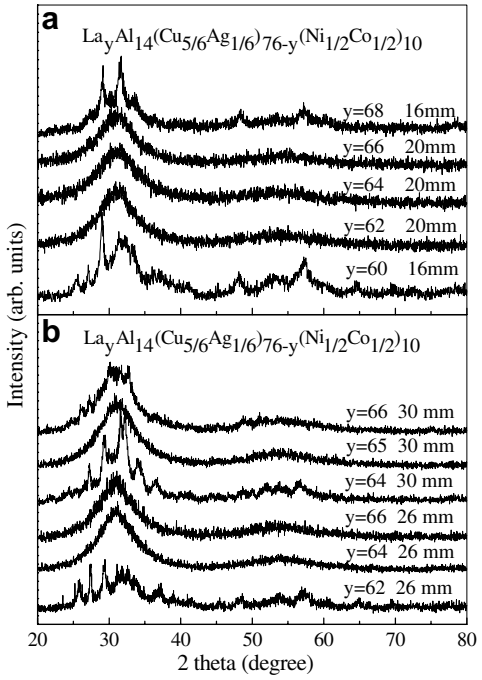

Fig. 2. XRD patterns of $La_yAl_{14}(Cu_{5/6}Ag_{1/6})_{76-y}(Ni_{1/2}Co_{1/2})_{10}$ ($y = 60$, 62, 64, 65, 66 and 68 at.%) pseudo-quaternary alloys with different diameters.

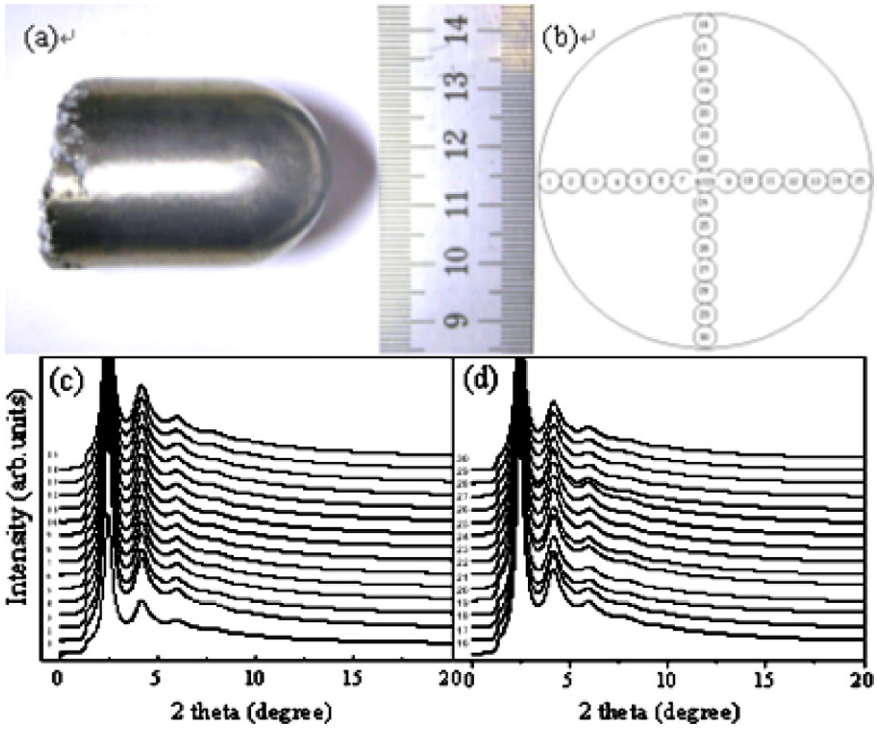

Fig. 3. A picture of an 30 mm amorphous $La_{65}Al_{14}(Cu_{5/6}Ag_{1/6})_{11}(Ni_{1/2}Co_{1/2})_{10}$ rod, together with its high-resolution X-ray diffraction patterns (c and d) recorded using 1×1 mm^2 beam size by synchrotron radiation at various positions (b).

Fig. 4 shows the DSC curves of the $La_yAl_{14}(Cu_{5/6}Ag_{1/6})_{76-y}(Ni_{1/2}Co_{1/2})_{10}$ ($y = 60, 62, 64, 65, 66$ and 68) glassy alloys. Table 1 lists the thermal parameters of these glassy rods, including the glass transition temperature (T_g), the onset crystallization temperature (T_{x1}), the melting temperature (T_m) and the liquidus temperature (T_l), as well as the supercooled liquid region, $\Delta T_x = T_{x1} - T_g$, the reduced glass transition temperature $T_{rg} = T_g/T_l$ and the γ value ($\gamma = T_{x1}/(T_g + T_l)$). Some other BMGs are also included for comparison [12,15]. As the composition changes from $y = 60$ to $y = 68$, both T_g and T_x decrease gradually from 426 K to 415 K for T_g and from 491 K to 418 K for T_x, respectively. The liquidus temperature T_l and the melting behavior are significantly affected by the composition. When the La content increases from 60 at.% ($y = 60$) to 68 at.% ($y = 68$), T_l first decreases from 743 K to 687 K then increases to 713 K, indicating the existence of a deep eutectic point in this composition range. These alloys exhibit relatively large ΔT_x, T_{rg} and γ values compared with the other Re-based amorphous alloys listed in Table 1 [12,15]. Comparing the thermal parameters of these alloys, it can be concluded that the high GFA, characterized by critical size D_c, is well reflected by the higher T_{rg} and γ values.

3.2. Thermal, kinetic and physical properties

The thermal stability of La-based BMGs is another key factor related to their use in engineering applications, which usually can be evaluated by examining the activation energy for crystallization of the BMGs. DSC measurements of the La-based BMGs prepared here were performed at different heating rates ($\phi = 5$–$8\ min^{-1}$). Obvious kinetic behaviors can be observed. As the heating rate increases, T_g, T_x and the crystallization peak shift to higher temperatures. Kissinger's equation is usually employed to evaluate the activation energy for glass transition of BMGs based on the glass transition temperatures at different heating rates ϕ [23]:

$$\ln\frac{T_g^2}{\phi} = \frac{E_a}{RT_g} + \text{const} \tag{5}$$

where R is the gas constant and E_a is the activation energy of glass transition. The Kissinger plots for the three alloys are presented in Fig. 5. The E_a values obtained for the $La_{62}Al_{14}Cu_{24}$, $La_{62}Al_{14}(Cu_{5/6}Ag_{1/6})_{24}$ and $La_{62}Al_{14}(Cu_{5/6}Ag_{1/6})_{14}(Ni_{1/2}Co_{1/2})_{10}$ alloys are 138, 153 and 193 kJ mol^{-1}, respectively, as listed in Table 2. Compared with

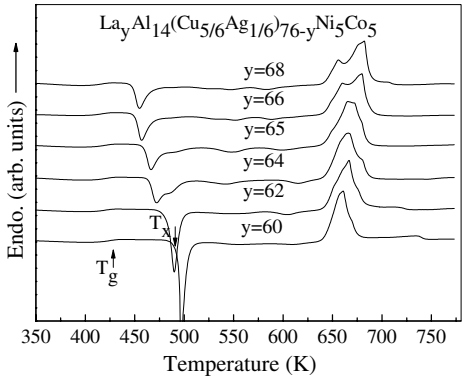

Fig. 4. DSC curves of the $La_yAl_{14}(Cu_{5/6}Ag_{1/6})_{76-y}(Ni_{1/2}Co_{1/2})_{10}$ ($y = 60, 62, 64, 65, 66$ and 68 at.%) glassy alloys.

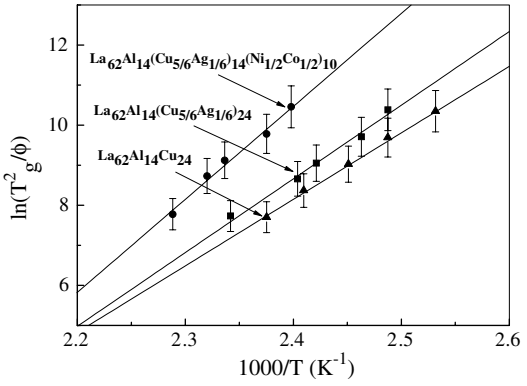

Fig. 5. Kissinger plots of T_g for the $La_{62}Al_{14}Cu_{24}$, $La_{62}Al_{14}(Cu_{5/6}Ag_{1/6})_{24}$ and $La_{62}Al_{14}(Cu_{5/6}Ag_{1/6})_{14}(Ni_{1/2}Co_{1/2})_{10}$ BMG alloys.

Table 1
The critical sizes (D_c) and thermal parameters for $La_{62}Al_{14}(Cu_{5/6}Ag_{1/6})_{24-x}(Ni_{0.5}Co_{0.5})_x$ ($x = 0, 4, 8, 10$ and 12 at.%) and $La_yAl_{14}(Cu_{5/6}Ag_{1/6})_{76-y}(Ni_{1/2}Co_{1/2})_{10}$ ($y = 60, 62, 64, 65, 66$ and 68 at.%) BMGs, together with some other BMGs reported in the literature for comparison

Compositions	D_c (mm)	T_g (K)	T_x (K)	T_m (K)	T_l (K)	ΔT_x (K)	T_{rg}	γ
$La_{62}Al_{14}Cu_{24}$	<5	401	449	673	734	48	0.546	0.396
$La_{62}Al_{14}Cu_{202}Ag_4$	8	404	456	656	729	52	0.554	0.402
$La_{62}Al_{14}(Cu_{5/6}Ag_{1/6})_{20}(Ni_{1/2}Co_{1/2})_4$	16–20	412	472	641	713	60	0.578	0.420
$La_{62}Al_{14}(Cu_{5/6}Ag_{1/6})_{16}(Ni_{1/2}Co_{1/2})_8$	16–20	415	477	640	708	62	0.586	0.425
$La_{62}Al_{14}(Cu_{5/6}Ag_{1/6})_{14}(Ni_{1/2}Co_{1/2})_{10}$	20–26	422	482	642	727	60	0.580	0.419
$La_{62}Al_{14}(Cu_{5/6}Ag_{1/6})_{12}(Ni_{1/2}Co_{1/2})_{12}$	16–20	429	471	644	698	42	0.615	0.418
$La_{60}Al_{14}(Cu_{5/6}Ag_{1/6})_{16}(Ni_{1/2}Co_{1/2})_{10}$	<16	426	491	642	743	65	0.573	0.420
$La_{62}Al_{14}(Cu_{5/6}Ag_{1/6})_{14}(Ni_{1/2}Co_{1/2})_{10}$	20–26	422	482	642	727	60	0.580	0.419
$La_{64}Al_{14}(Cu_{5/6}Ag_{1/6})_{12}(Ni_{1/2}Co_{1/2})_{10}$	26	421	464	642	687	43	0.613	0.419
$La_{65}Al_{14}(Cu_{5/6}Ag_{1/6})_{11}(Ni_{1/2}Co_{1/2})_{10}$	30	419	459	641	687	40	0.610	0.415
$La_{66}Al_{14}(Cu_{5/6}Ag_{1/6})_{10}(Ni_{1/2}Co_{1/2})_{10}$	26	415	450	641	690	35	0.601	0.407
$La_{68}Al_{14}(Cu_{5/6}Ag_{1/6})_8(Ni_{1/2}Co_{1/2})_{10}$	<16	415	448	642	713	33	0.582	0.397
$La_{62}Al_{14}(Cu_{0.5}Ni_{0.5})_{24}$ [16]	1.2	423	452	684	744	29	0.57	0.387
$(CeLaPrNd)_{65}Co_{25}Al_{10}$ [17]	1.5	431	455	701	729	24	0.59	0.402

Table 2
The parameters obtained from the heating rate dependence of the onset of crystallization temperature and glass transition temperature, including the activation energy E_a, T_0, strength parameter D, ln$B$ and fragility index m ($La_{62}Al_{14}Cu_{24}$, $La_{62}Al_{14}(Cu_{5/6}Ag_{1/6})_{24}$ and $La_{62}Al_{14}(Cu_{5/6}Ag_{1/6})_{14}(Ni_{1/2}Co_{1/2})_{10}$ alloys are labeled A, B and C, respectively)

Alloys	E_a (kJ mol^{-1})	T_0 (K)	D	ln B	m
A	138	359	0.66	7.87	17
B	153	371	0.53	7.88	20
C	193	376	0.83	9.30	22

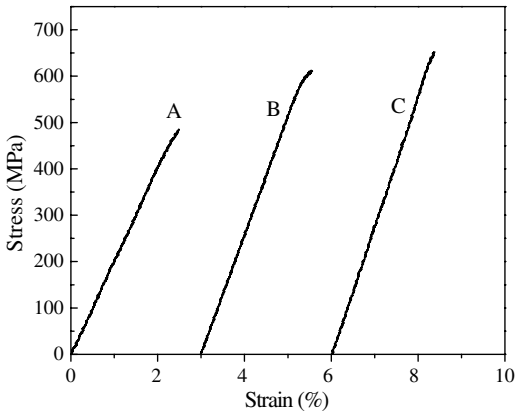

Fig. 6. Compressive stress–strain curves of as-cast glassy rods with 2 mm in diameter and 4 mm in length at a strain rate of 4×10^{-4} s^{-1} at room temperature: (A) $La_{62}Al_{14}Cu_{24}$, (B) $La_{62}Al_{14}(Cu_{5/6}Ag_{1/6})_{24}$ and (C) $La_{62}Al_{14}(Cu_{5/6}Ag_{1/6})_{14}(Ni_{1/2}Co_{1/2})_{10}$.

other BMGs [24–26], the newly developed La-based BMG alloys show relatively smallerE_a values. The larger the E_a value, the greater the thermal stability of the alloy. It seems that the $La_{62}Al_{14}(Cu_{5/6}Ag_{1/6})_{14}(Ni_{1/2}Co_{1/2})_{10}$ alloy has the greatest thermal stability of the La-based BMG alloys developed here.

Fig. 6 shows compressive stress–strain curves of the as-cast $La_{62}Al_{14}Cu_{24}$, $La_{62}Al_{14}(Cu_{5/6}Ag_{1/6})_{24}$ and $La_{62}Al_{14}(Cu_{5/6}Ag_{1/6})_{14}Ni_5Co_5$ glassy rods at a strain rate of 4×10^{-4} s^{-1}. It is found that the Ag and Ni–Co substitutions significantly enhance the fracture strength of the $La_{62}Al_{14}(Cu_{5/6}Ag_{1/6})_{24}$ and $La_{62}Al_{14}(Cu_{5/6}Ag_{1/6})_{14}Ni_5Co_5$ alloys, from 480 MPa for the ternary $La_{62}Al_{14}Cu_{24}$ to 610 and 650 MPa, respectively. No significant plastic deformation was detected in the developed La-based BMG alloys. The $La_{62}Al_{14}(Cu_{5/6}Ag_{1/6})_{14}Ni_5Co_5$ alloy also shows a Vicker's hardness of about 200 kg mm^{-2}. Ultrasonic measurements were carried out to determine the elastic constants of amorphous $La_{62}Al_{14}(Cu_{5/6}Ag_{1/6})_{14}Ni_5Co_5$ alloy with density $\rho = 6.19$ g cm^{-3}. The Young's modulus, shear modulus, bulk modulus and Poisson ratio were determined to be 35, 13, 41 and 0.356 GPa, respectively.

4. Discussion

A number of factors, including atomic size mismatch, thermodynamics and kinetics, play important roles in determining the GFA of metallic glasses [1–3,27–33]. To further understand the origin of high GFA in the La–Al–(Cu, Ag)–(Ni, Co) pseudo-quaternary alloy system, a systematical comparison in terms of the fragility index and structural and thermodynamic factors was carried out between the $La_{62}Al_{14}Cu_{24}$, $La_{62}Al_{14}(Cu_{5/6}Ag_{1/6})_{24}$ and $La_{62}Al_{14}(Cu_{5/6}Ag_{1/6})_{14}(Ni_{1/2}Co_{1/2})_{10}$ BMG alloys.

The well-known fragility parameter could be used to classify glass forming liquid as strong or fragile [30]. Generally, a strong liquid usually has a higher viscosity at its melting point than a fragile one. The smaller the m value, the stronger the glass former [34]. There are several approaches to quantifying the value of the fragility parameter m defined as [35]:

$$m = \left.\frac{\mathrm{d}\log(\tau)}{\mathrm{d}(T_g/T)}\right|_{T=T_g} \tag{6}$$

where τ is the average relaxation time and T is the temperature. Here, m can be calculated using the Vogel–Fulcher equation [36]:

$$\ln\phi = \ln B - \frac{DT_0}{T_g - T_0} \tag{7}$$

where B is the time scale parameter in the glass forming system, D is the strength parameter in the VFT equation and T_0 describes the onset of the glass transition in the limit

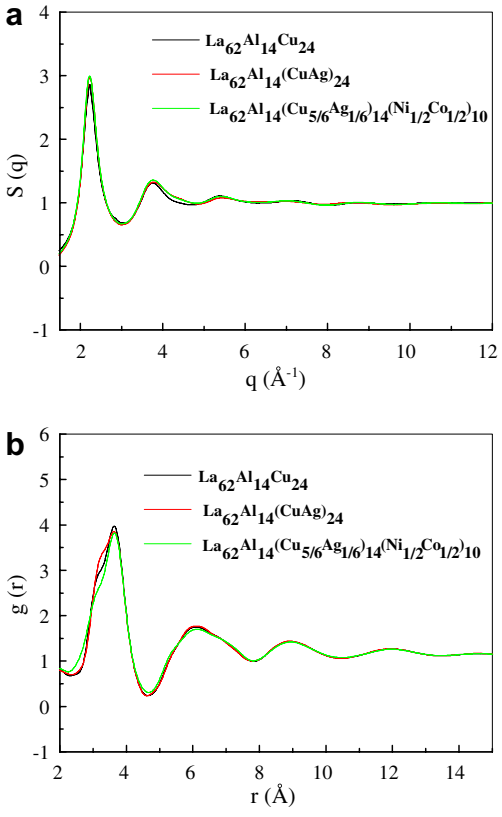

Fig. 7. (a) Structure factor $S(q)$ and (b) pair distribution function $g(r)$ for the glassy $La_{62}Al_{14}Cu_{24}$, $La_{62}Al_{14}(Cu_{5/6}Ag_{1/6})_{24}$ and $La_{62}Al_{14}(Cu_{5/6}Ag_{1/6})_{14}(Ni_{1/2}Co_{1/2})_{10}$ alloys at room temperature.

of ϕ close to 0. These parameters could be obtained from the heating rate dependence of the glass transition temperature. The fitted parameters are given in Table 2. The fitted D and T_0 could be used to calculate the fragility index m based on the following equation [37]:

$$m = \frac{DT_0T_g}{(T_g - T_0)^2 \ln 10} \tag{8}$$

The fragility index m is listed in Table 2. The m values of the present alloys are quite consistent with previous m values reported by Lu et al. for a similar alloy system [38]. However, among the three samples studied here, the pseudo-quaternary $La_{62}Al_{14}(Cu_{5/6}Ag_{1/6})_{14}Ni_5Co_5$ alloy has the highest m value and also the highest GFA compared with other two alloys. This phenomenon was also found in Pd-based BMGs [34]. This would suggest that the fragility index m does not explain the glass-forming ability of

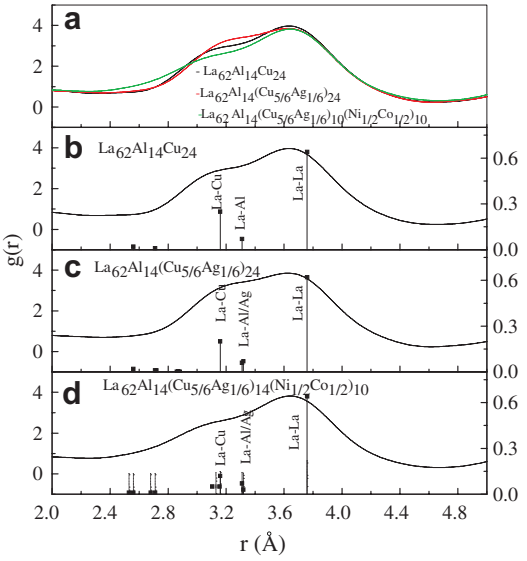

Fig. 8. The first peaks of pair distribution function $g(r)$ for the glassy alloys. (a) Difference between the three alloys; (b) $La_{62}Al_{14}Cu_{24}$; (c) $La_{62}Al_{14}(Cu_{5/6}Ag_{1/6})_{24}$ and and (d) $La_{62}Al_{14}(Cu_{5/6}Ag_{1/6})_{14}(Ni_{1/2}Co_{1/2})_{10}$. The bars indicate the interatomic distances from the hard sphere model. The height of the bars corresponds to the partial structure factor weight values.

$La_{62}Al_{14}Cu_{24}$, $La_{62}Al_{14}(Cu_{5/6}Ag_{1/6})_{24}$, and $La_{62}Al_{14}(Cu_{5/6}Ag_{1/6})_{14}Ni_5Co_5$ alloys.

Numerous structural investigations have been carried out to probe the origin of the glass forming ability of BMGs [27,39–41]. In the present alloy system, the atomic radii of components are La 0.188 nm, Al 0.143 nm, Cu 0.128 nm, Ag 0.144 nm, Ni 0.125 nm and Co 0.125 nm [39]. The ratios of atomic radii are estimated to be $R_{Al/La} = 0.761$, $R_{Cu/La} = 0.680$, $R_{Ag/La} = 0.766$, $R_{Ni/La} = 0.665$ and $R_{Co/La} = 0.665$. The heat-of-mixing values of La–Al, La–Cu, La–Ag, La–Ni and La–Co are −38, −21, −30, −27, and −17 kJ mol^{-1}, respectively [42]. It is proposed that the large negative heat-of-mixing values and intermediate atomic mismatches enhance the interactions between the components and the local random packing density [2]. Fig. 7 presents the structure factor $S(q)$ in Fig. 7a and the pair correlation function $g(r)$ in Fig. 7b for the glassy $La_{62}Al_{14}Cu_{24}$, $La_{62}Al_{14}(Cu_{5/6}Ag_{1/6})_{24}$ and $La_{62}Al_{14}(Cu_{5/6}Ag_{1/6})_{14}(Ni_{1/2}Co_{1/2})_{10}$ alloys at room temperature according to the following equations [43]:

$$G(r) = 4\pi r[(\rho(r) - \rho_0)] = \frac{2}{\pi}\int_0^\infty Q \cdot I(Q) \cdot \sin(Qr)\mathrm{d}Q \tag{9}$$

$$g(r) = \frac{\rho(r)}{\rho_0} = 1 + \frac{G(r)}{4\pi r\rho_0} \tag{10}$$

where $\rho(r)$ is the radial density function and ρ_0 is the average atomic number density. It can be seen from Fig. 7a and b that both the peak positions and profiles in the $S(q)$ and $g(r)$ curves of the pseudo-ternary La–Al–(Cu, Ag) alloys and quaternary La–Al–(Cu, Ag)–(Ni, Co) alloys are quite analogous to those of La–Al–Cu alloys. Differences in the first broad peak of radial distribution functions for the three BMG alloys can be detected in Fig. 8a. A hard sphere model using the nominal atomic radii was employed to interpret the tiny difference in the first $g(r)$ peak. The distance between two atoms based on a hard sphere model and calculated partial radial distribution function weight values for $La_{62}Al_{14}Cu_{24}$,$La_{62}Al_{14}(Cu_{5/6}Ag_{1/6})_{24}$ and $La_{62}Al_{14}(Cu_{5/6}Ag_{1/6})_{14}(Ni_{1/2}Co_{1/2})_{10}$ alloys are listed in Table 3 and also indicated in Fig. 8b–d. It is found that La–La, La–Cu and La–Al dominate the first peak. However, as the weight value of La–Cu decreases and those of La–Ag and La–(NiCo) new pairs increase due to Ag

Table 3
Interatomic distance between two atoms based on the hard sphere model and calculated partial radial distribution function weights for (A) $La_{62}Al_{14}Cu_{24}$, (B) $La_{62}Al_{14}(Cu_{5/6}Ag_{1/6})_{24}$ and (C) $La_{62}Al_{14}(Cu_{5/6}Ag_{1/6})_{14}(Ni_{1/2}Co_{1/2})_{10}$ alloys

Bond type		La–La	La–Al	La–Cu	La–Ag	La–Ni	La–Co	Al–Al	Al–Cu	Al–Ag	Al–Ni	Al–Co
Distance	(Å)	3.76	3.31	3.16	3.32	3.13	3.13	2.86	2.71	2.87	2.68	2.68
Weight factor	A	0.64	0.07	0.25				0.002	0.01			
	B	0.62	0.06	0.20	0.07			0.002	0.01	0.003		
	C	0.64	0.07	0.12	0.03	0.05	0.05	0.002	0.01	0.001	0.003	0.003
Bond type		Cu–Cu	Cu–Ag	Cu–Ni	Cu–Co	Ag–Ag	Ag–Ni	Ag–Co	Ni–Ni	Ni–Co	Co–Co	
Distance	(Å)	2.56	2.72	2.53	2.53	2.88	2.69	2.69	2.5	2.5	2.5	
Weight factor	A	0.02										
	B	0.02	0.01			0.002						
	C	0.01	0.003	0.005	0.005	0.0003	0.001	0.001	0.001	0.002	0.0009	

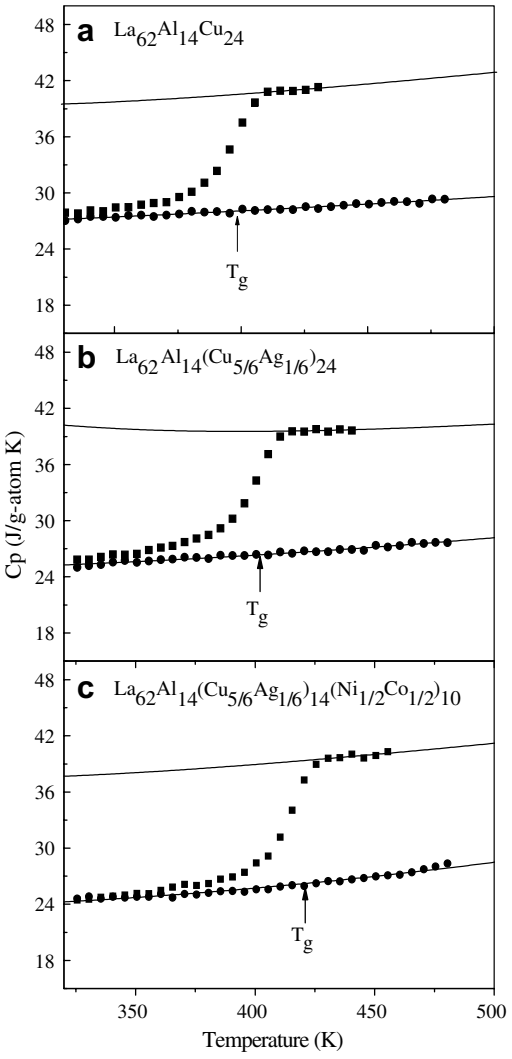

Fig. 9. Specific heat capacities (C_p) of (a) $La_{62}Al_{14}Cu_{24}$, (b) $La_{62}Al_{14}(Cu_{5/6}Ag_{1/6})_{24}$ and (c) $La_{62}Al_{14}(Cu_{5/6}Ag_{1/6})_{14}(Ni_{1/2}Co_{1/2})_{10}$ alloys measured in the crystalline, supercooled liquid and amorphous states.

and Ni–Co substitution, the shoulder at $r = 3.3$ Å first increases and then decreases, while the $g(r)$ at $r = 2.5$–2.7 Å increases gradually due to various contributions of Cu–Ni and Cu–Co. As far as the area of the first peak in $g(r)$ is concerned, there is no obvious increase in the coordination number between the three BMG alloys. Consequently, although Ag and Ni–Co substitution of Cu atoms does not affect the first coordination number greatly, it is most likely that the local random packing becomes denser due to multi-elements with similar atomic sizes, e.g. the Ag atom size is similar to that of Al, and Ni and Co are similar to Cu.

From the kinetic and structural points of view, there is little evidence that could explain the origin of the high GFA of the present alloy system. The differences in thermodynamic parameters, including the enthalpy change $\Delta H_{l\text{–}s}(T)$, entropy change $\Delta S_{l\text{–}s}(T)$ and Gibbs free-energy difference $\Delta G_{l\text{–}s}(T)$, between the supercooled liquid state and the crystalline states were further investigated by measuring the specific heat capacities of the three alloys. Fig. 9 shows the specific heat capacities of three $La_{62}Al_{14}Cu_{24}$, $La_{62}Al_{14}(Cu_{5/6}Ag_{1/6})_{24}$ and $La_{62}Al_{14}(Cu_{5/6}Ag_{1/6})_{14}(Ni_{1/2}Co_{1/2})_{10}$ alloys that were measured in the crystalline, supercooled liquid and amorphous states. These specific heat capacity data of the undercooled liquid and the crystal are usually fitted using the following relationships [28,34]:

$$C_p^s = 3R + aT + bT^2 \tag{11}$$

$$C_p^l = 3R + cT + dT^{-2} \tag{12}$$

where $R = 8.3142$ J g atom^{-1} K^{-1} and a, b, c, and $d$are fitting constants. Table 4 lists the fitting results together with heat of fusion ΔH_m and the entropy of fusion $\Delta S_m = \Delta H_m/T_m$ at the melting point T_m for the $La_{62}Al_{14}Cu_{24}$,$La_{62}Al_{14}(Cu_{5/6}Ag_{1/6})_{24}$ and $La_{62}Al_{14}(Cu_{5/6}Ag_{1/6})_{14}(Ni_{1/2}Co_{1/2})_{10}$ alloys studied in this work.

The thermodynamic parameters, including the enthalpy change $\Delta H_{l\text{–}s}(T)$, entropy change $\Delta S_{l\text{–}s}(T)$ and Gibbs free-energy difference $\Delta G_{l\text{–}s}(T)$, of the undercooled liquid with respect to the crystal can be calculated by integrating the specific heat capacity difference with the respective values at T_m:

$$\Delta H_{l\text{–}s}(T) = \Delta H_m - \int_T^{T_m} [C_p^l(T) - C_p^s(T)]dT \tag{13}$$

$$\Delta S_{l\text{–}s}(T) = \Delta S_m - \int_T^{T_m} \frac{C_p^l(T) - C_p^s(T)}{T} dT \tag{14}$$

$$\Delta G_{l\text{–}s}(T) = \Delta H_m - \int_T^{T_m} [C_p^l(T) - C_p^s(T)]dT - \Delta S_m T + T\int_T^{T_m} \frac{C_p^l(T) - C_p^s(T)}{T} dT \tag{15}$$

Fig. 10 shows the enthalpy change $\Delta H_{l\text{–}s}(T)$ and entropy change $\Delta S_{l\text{–}s}(T)$ of the undercooled liquid with respect to the crystalline phase as a function of temperature. Generally, for an alloy, the enthalpy of supercooled liquid

Table 4
Fitting parameters from the heat capacity data, using $C_p^s = 3R + aT + bT^2$ to fit the crystalline state heat capacity data and $C_p^l = 3R + cT + dT^{-2}$ to fit the liquid heat capacity data, together with the melting point T_m, the heat of fusion ΔH_m, the entropy of fusion $\Delta S_m = \Delta H_m/T_m$, the Kauzmann temperature T_K and the coordination number N for the $La_{62}Al_{14}Cu_{24}$, $La_{62}Al_{14}(Cu_{5/6}Ag_{1/6})_{24}$ and $La_{62}Al_{14}(Cu_{5/6}Ag_{1/6})_{14}(Ni_{1/2}Co_{1/2})_{10}$ alloys (labeled as A, B and C, respectively)

Alloys	a (J mol^{-1} K^{-1})	b (J mol^{-1} K^{-1})	c (J mol^{-1} K^{-1})	d (J mol^{-1} K^{-1})	T_m (K)	ΔH_m (kJ mol^{-1})	ΔS_m (J mol^{-1} K^{-1})	T_k (K)
A	0.00189	1.49×10^{-5}	0.0326	4.16×10^5	673	6.835	10.156	312
B	−0.00869	3.04×10^{-5}	0.024739	7.54×10^5	656	6.118	9.326	314
C	−0.0186	5.14×10^{-5}	0.029944	3.24×10^5	637	5.602	8.795	317

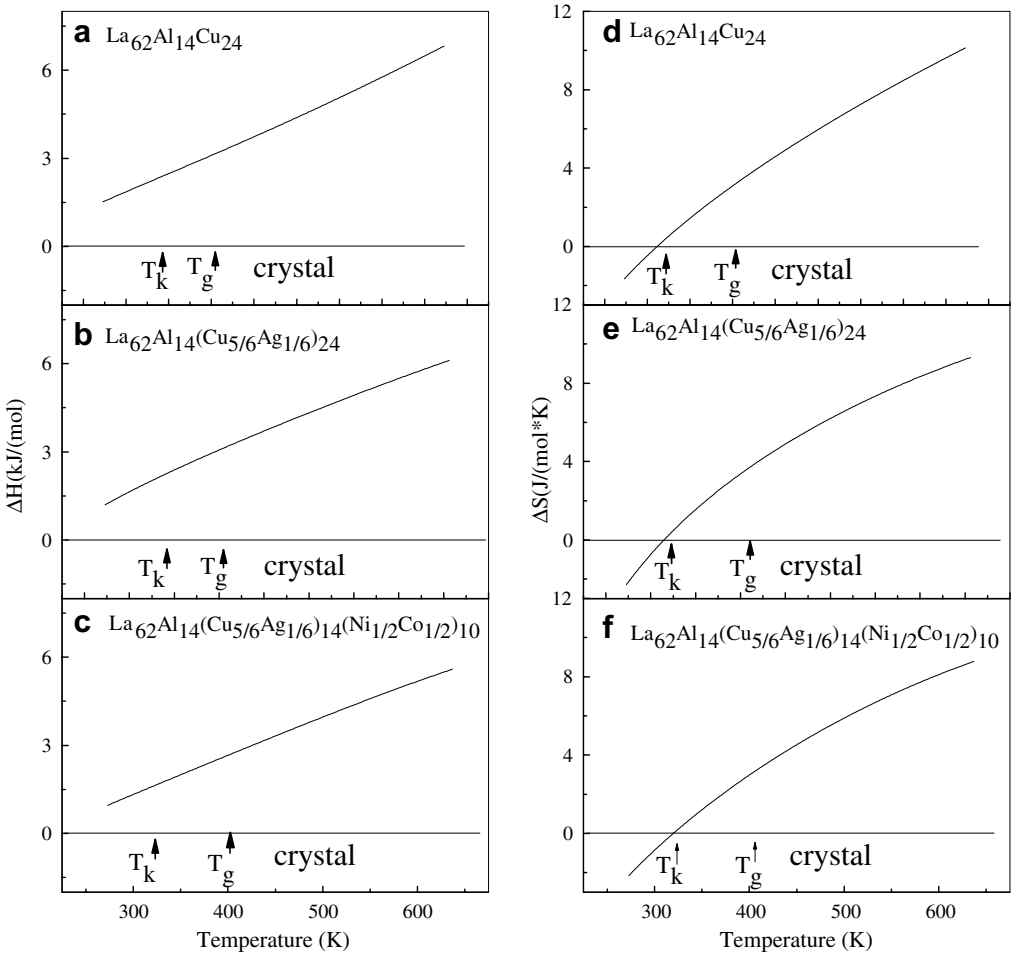

Fig. 10. Enthalpy change $\Delta H_{l-s}(T)$ and entropy change $\Delta S_{l-s}(T)$ of the undercooled liquid with respect to the crystal of (a, d) $La_{62}Al_{14}Cu_{24}$, (b, e) $La_{62}Al_{14}(Cu_{5/6}Ag_{1/6})_{24}$ and (c, f) $La_{62}Al_{14}(Cu_{5/6}Ag_{1/6})_{14}(Ni_{1/2}Co_{1/2})_{10}$ alloys, respectively. Kauzmann temperatures T_K for the three alloys are indicated by arrows in the plots.

decreases more slowly than the entropy. Therefore, the entropy crisis is first faced upon cooling if no glass transition occurs. The Kauzmann temperature T_K is an isenthalpic and isentropic temperature at which the entropy of a liquid is equal to the entropy of the crystalline form [34]. Here, the calculated T_K of the three alloys indicated on the plots is determined to be 312 K for the $La_{62}Al_{14}Cu_{24}$ alloy, 314 K for the $La_{62}Al_{14}(Cu_{5/6}Ag_{1/6})_{24}$ alloy and 317 K for the $La_{62}Al_{14}(Cu_{5/6}Ag_{1/6})_{14}(Ni_{1/2}Co_{1/2})_{10}$ alloy. This temperature is commonly believed to be the lowest temperature at which a supercooled liquid can exist without spontaneous crystallization or a glass formation [29].

To compare the driving force of crystallization for the three La-based alloys, the excess Gibbs free-energy differences as a function of temperature normalized to the melting point of the corresponding alloy are plotted in Fig. 11. For the present three La-based BMGs, the Gibbs free-energy differences at T_k range from 1.5 kJ mol^{-1} for $La_{62}Al_{14}(Cu_{5/6}Ag_{1/6})_{14}(Ni_{1/2}Co_{1/2})_{10}$ to 2.0 kJ mol^{-1} for $La_{62}Al_{14}Cu_{24}$ alloy. Compared with the values reported for Pd-, Zr-, Mg-, Pt-based BMGs, the three La-based BMGs exhibit relatively smaller driving force for crystallization, which implies their high glass forming ability. However, among these three La-based BMGs, the difference in Gibbs free energy for La–Al–Cu alloy is the largest, so that only 2 mm fully glassy rods can be formed [12]. Ag addition slightly decreases the Gibbs free-energy difference of the La–Al–(Cu, Ag) alloy, resulting in an increased GFA.

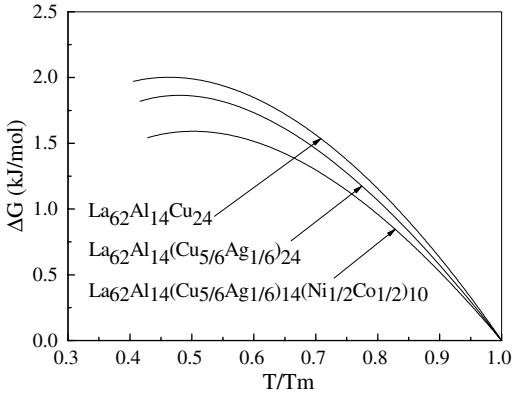

Fig. 11. Gibbs free-energy difference $\Delta G_{l-s}(T)$ of the undercooled liquid with respect to the crystal of (a) $La_{62}Al_{14}Cu_{24}$, (b) $La_{62}Al_{14}(Cu_{5/6}Ag_{1/6})_{24}$ and (c) $La_{62}Al_{14}(Cu_{5/6}Ag_{1/6})_{14}(Ni_{1/2}Co_{1/2})_{10}$ alloys.

Furthermore, with the introduction of Ni and Co atoms, $La_{62}Al_{14}(Cu_{5/6}Ag_{1/6})_{14}(Ni_{1/2}Co_{1/2})_{10}$ alloy shows the lowest Gibbs free-energy difference and exhibits the highest GFA. Therefore, the small driving force for crystallization of La–Al–(Cu,Ag)–(Ni, Co) alloys turns out to be one crucial factor in interpreting their higher GFA with Ag and Ni–Co substitution.

5. Conclusions

The optimal composition for high glass forming pseudo-quaternary La–Al–(Cu, Ag)–(Ni, Co) BMGs has been carefully studied. The results obtained can be summarized as follows:

(1) Fully glassy rods 20 mm in diameter can be fabricated in a wide composition range by using the copper mold casting method. However, the GFA is strongly sensitive to the composition. With only a 3 at.% increased La content, the critical size of $La_{65}Al_{14}(Cu_{5/6}Ag_{1/6})_{11}(Ni_{1/2}Co_{1/2})_{10}$ BMG increases to 30 mm, compared with 20 mm for $La_{62}Al_{14}(Cu_{5/6}Ag_{1/6})_{14}(Ni_{1/2}Co_{1/2})_{10}$ BMG.

(2) The best composition for glass formation was found to be around $La_{65}Al_{14}(Cu_{5/6}Ag_{1/6})_{11}(Ni_{1/2}Co_{1/2})_{10}$, for which 30 mm fully amorphous rods can be successfully fabricated by the water quenching method. It has the highest GFA of all the Re-based alloys reported so far.

(3) The La-based BMG alloys developed here exhibit rather low glass transition temperatures T_g and relatively wide supercooled liquid regions; for example, for $La_{62}Al_{14}(Cu_{5/6}Ag_{1/6})_{14}(Ni_{1/2}Co_{1/2})_{10}$ BMG, $T_g = 422$ K, $\Delta T_x = 60$ K, fracture strength = 650 GPa, Vicker's hardness = 200 kg mm^{-2}, density $\rho = 6.19$ g cm^{-3}, Young's modulus = 35 GPa, shear modulus = 13 GPa, and Poisson's ratio = 0.356.

(4) Finally, the origin of high GFA enhanced by Ag and Ni–Co substitution in the La–Al–Cu system was investigated. The low Gibbs free-energy difference between amorphous and crystalline La–Al–(Cu, Ag)–(Ni, Co) alloys turns out to be one key factor in interpreting its high GFA, whereas no obvious relationship is observed between GFA and the fragility index m.

Note added in proof

While this paper was under review, we further performed Cu-mold casting experiments and found the critical size for forming BMG to be 35 mm for the $La_{65}Al_{14}(Cu_{5/6}Ag_{1/6})_{11}(Ni_{1/2}Co_{1/2})_{10}$ alloy.

Acknowledgements

The authors thank BSRF in Beijing, and NSRL in Hefei, China; HASYLAB in Hamburg, Germany; MAX–Lab in Lund, Sweden; KEK and SPring8 in Japan for use of the synchrotron radiation facilities. Financial support from the National Natural Science Foundation of China (Grants Nos. 50341032, 50425102 and 50601021), the Ministry of Science and Technology of China (Grant Nos. 2004/249/37-14 and 2004/250/31-01A), the Ministry of Education of China, Zhejiang University–Helmholtz cooperation fund, Zhejiang University and the EU project (Ductile BMG Composites MRTN-CT-2003-504692) is gratefully acknowledged.

References

[1] Greer AL. Science 1995;267:1947.
[2] Inoue A. Acta Mater 2000;48:279.
[3] Johnson WL. MRS Bull 1999;24:42.
[4] Ma H, Shi LL, Xu J, Li Y, Ma E. Appl Phys Lett 2005;87:181915.
[5] Nishiyama N, Inoue A. Mater Trans JIM 1996;37:1531.
[6] Peker A, Johnson WL. Appl Phys Lett 1993;63:2342.
[7] Guo F, Poon SJ, Shiflet GJ. Appl Phys Lett 2003;83:2675.
[8] He Y, Price CE, Poon SJ, Shiflet GJ. Philos Mag Lett 1994;70:371.
[9] Zhao ZF, Zhang Z, Wang WH. Appl Phys Lett 2003;82:4699.
[10] Zhang B, Zhao DQ, Pan MX, Wang WH, Greer AL. Phys Rev Lett 2005;94:205502.
[11] Jiang QK, Zhang GQ, Chen LY, Jiang JZ. J Alloy Compd 2006;424:179.
[12] Li R, Pang SJ, Men H, Ma CL, Zhang T. Scripta Mater 2006;54:1123.
[13] Inoue A, Yamaguchi H, Zhang T, Masumoto T. Mater Trans JIM 1990;31:104.
[14] Tan H, Lu ZP, Yao HB, Yao B, Feng YP, Li Y. Mater Trans 2001;42(4):268.
[15] Zhang Y, Tan H, Li Y. Mater Sci Eng A 2004;436:375.
[16] Han T, Zhang Y, Ma D, Feng YP, Li Y. Acta Mater 2003;51:4551.
[17] Jiang QK, Zhang GQ, Chen LY, Wu JZ, Zhang HG, Jiang JZ. J Alloy Compd 2006;424:183.
[18] Bouchard R, Hupfeld D, Lippmann T, Neuefeind J, Neumann HB, Poulsen HF, et al. Synchrotron Radiat 1998;5:90.
[19] Hammersley AP, Svensson SO, Hanfland M, Fitch AN, Häusermann D. High Press Res 1996;14:235.
[20] Jeong IK, Thompson J, Turner AMP, Billinge SJL. J. Appl Crystallogr 2001;34:536.
[21] Zhang B, Wang RJ, Zhao DQ, Pan MX, Wang WH. Phys Rev B 2006;73:092201.
[22] Schreiber D. Elastic Constants and Measurement. New York: McGraw-Hill; 1973.
[23] Kissinger HE. Anal Chem 1957;29:1702.
[24] Mitrovic N, Roth S, Eckert J. Appl Phys Lett 2001;78:2145.
[25] Li Z, Bai HY, Pan MX, Wang WH. J Mater Res 2003;18:2208.
[26] Nishiyama N, Inoue A. Acta Mater 1999;47:1487.
[27] Miracle DB. Nat Mater 2004;3:697.
[28] Busch R, Kim YJ, Johnson WL. J Appl Phys 1995;77:4039.
[29] Glade SC, Busch R, Lee DS, Johnson WL, Wunderlich RK, Fecht HJ. J Appl Phys 2000;87:7242.
[30] Angell CA. Science 1995;267:1924.
[31] Mukherjee S, Schroers J, Zhou Z, Johnson WL, Rhim WK. Acta Mater 2004;52:3689.
[32] Mukherjee S, Schroers J, Johnson WL, Rhim WK. Phys Rev Lett 2005;94:245501.
[33] Legg BA, Schroers J, Busch R. Acta Mater 2007;55:1109.
[34] Fan GJ, Loffler JF, Wunderlich RK, Fecht HJ. Acta Mater 2004;52:667.
[35] Bohmer R, Angell CA. Phys Rev B 1992;45:10091.
[36] Bruning R, Samwer K. Phys Rev B 1992;46:11318.
[37] Bohmer R, Ngai KL, Angell CA, Plazek DJ. J Chem Phys 1993;99:4201.

[38] Lu ZP, Li Y, Liu CT. J Appl Phys 2003;93:286.
[39] Miracle DB, Sanders WS, Senkov ON. Phil Mag A 2003;83:2409.
[40] Inoue A. Bulk Amorphous Alloys, Practical Characteristics and Applications, Materials Science Foundation. Zurich:Trans Tech Publications.
[41] Sheng HW, Luo WK, Alamgir FM, Bai JM, Ma E. Nature 2006;439(7075):419.
[42] Boerde FR, Boom R, Matterns WCM, Miedema AR, Niessen AK. Cohesion in Metals. Amsterdam: North-Holland; 1998.
[43] Yavari AR, Moulec AL, Inoue A, Nishiyama N, Lupu N, Matsubara E, et al. Acta Mater 2005;53:1611.